Discovery of a potential allosteric ligand binding site in CDK2

Stephane Betzi, Riazul Alam, Mathew Martin, Donna J. Lubbers, Huijong Han, Sudhakar R. Jakkaraj, Gunda I. Georg and Ernst Schönbrunn

SUPPORTING INFORMATION

Supplementary Table 1 Summary of data collection and refinement of additional crystal structures determined as part of this work. Values in parentheses refer to the highest resolution shells.

Structure (PDB ID)	APO (3PXR)	3 ANS MOLECULES (3PXQ)	JWS648 (3PXY)	SU9516 (3PY0)
Crystallization				
Precipitant	Jeffamine ED-2001	PEG 3350	PEG 3350	PEG 3350
Co-crystallization	-	-	JWS648	SU9516
Soaking	-	ANS (15 mM)	-	-
Data Collection				
Space group	$P2_12_12_1$	$P2_12_12_1$	$P2_12_12_1$	$P2_12_12_1$
Unit cell dimensions: a, b, c (Å)	a=53.5 b=72.1 c=71.9	a=52.8 b=69.7 c=72.3	a=52.8 b=71.7 c=72.1	a=53.5 b=71.9 c=72.3
Resolution range	20-2.00 (2.05-2.00)	20-1.9 (1.95-1.9)	20-1.80 (1.85-1.80)	20-1.75 (1.80-1.75)
Unique reflections	19243(1353)	21475 (1528)	25605(1984)	28701(2316)
Completeness (%)	99.3 (99.7)	99.2 (96.0)	98.3 (97.2)	99.5 (99.8)
I/σI	17 (4.3)	38 (9.0)	21 (6.3)	18 (5.0)
R_{merge}[a] (%)	5.5 (28.4)	2.4 (9.1)	4.7 (23.9)	5.0 (27.4)
Structure refinement				
Protein atoms **Average B-factor (Å^2)**	2368 27	2399 24	2394 28	2388 31
Ligand(s) atoms **Average B-factor (Å^2)**	0 NA	63 24	17 25	18 23
Solvent molecules **Average B-factor (Å^2)**	153 30	213 39	179 31	183 35
Rmsd[b] bonds (Å)	0.010	0.010	0.008	0.010
Rmsd angles (°)	1.4	1.4	1.4	1.5
R_{cryst}[c] (%)	20.1	19.6	21.1	21.2
R_{free}[d] (%)	23.5	23.5	24.2	26.0
R_{free} reflection set size	963 (5%)	1096 (5.1%)	1025 (4.0%)	1091 (3.8%)
Cross-validated coordinate error:				
- From Luzzati plot (Å)	0.26	0.25	0.25	0.26
- From SigmaA (Å)	0.01	0.13	0.17	0.17

[a] $R_{merge} = 100 \times \Sigma_h\Sigma_i |I_{hi} - I_h| / \Sigma_{hi}I_{hi}$ where h are unique reflection indices.
[b] Rmsd = root mean square deviation from ideal values.
[c] $R_{cryst} = 100 \times \Sigma | F_{obs}-F_{model} | / F_{obs}$ where F_{obs} and F_{model} are observed and calculated structure factor amplitudes, respectively.
[d] R_{free} is R_{cryst} calculated for randomly chosen unique reflections, which were excluded from the refinement.

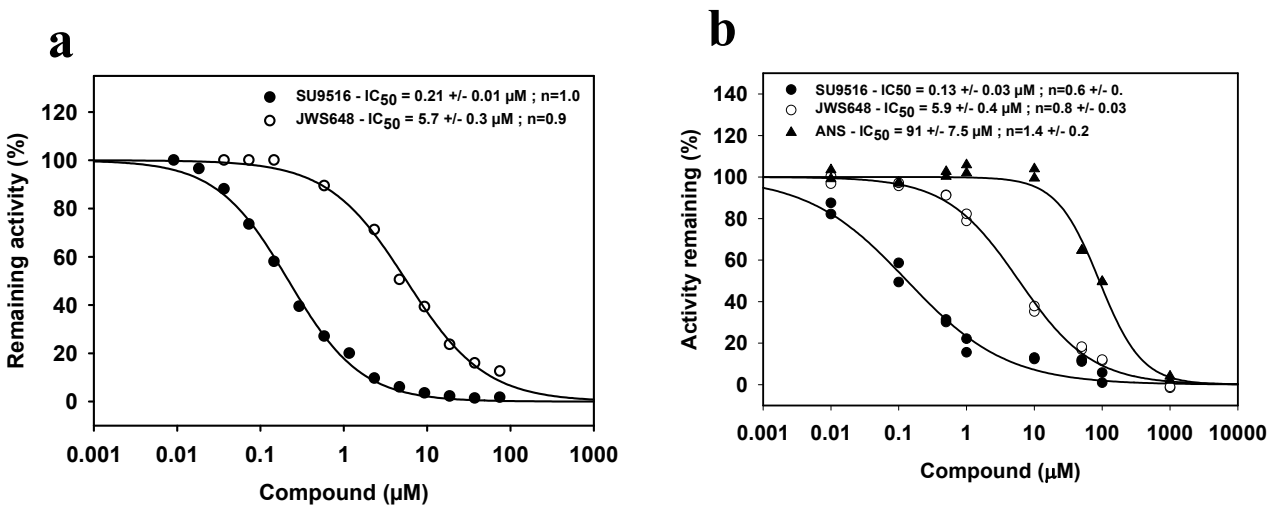

Supplementary Figure 1 Evaluation of the inhibitory potential of ANS on the activated CDK2-cyclin A2 complex.
(a) The IC50 values for the ATP-site directed inhibitors JWS648 (○) and SU9516 (●) were first determined using the PK-LDH coupled activity assay. (b) Due to the absorbance of ANS at 340 nm a different fluorescence-based coupled activity assay was employed, which resulted in comparable IC50 values for the inhibitors and revealed inhibition of CDK2 by ANS (▲) with an IC50 value of 91 µM. Data were fitted to equation (1). Details for the activity assays are described in the Methods section.

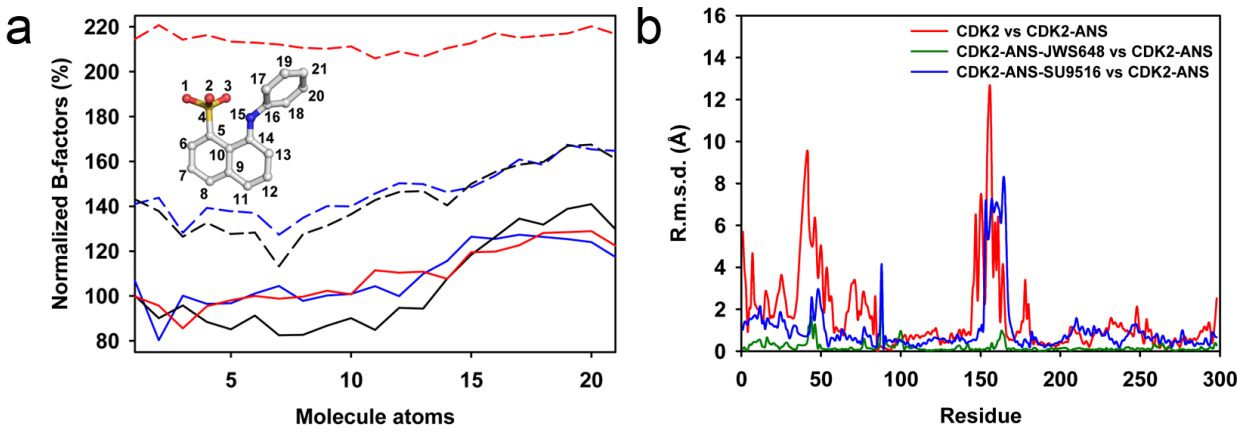

Supplementary Figure 2 Structure analysis of the binary and ternary CDK2-ANS complexes. **a**) Normalized B-factor analysis of ANS molecules bound to CDK2-ANS (black), CDK2-ANS-JWS648 (blue), and CDK2-ANS-SU9516 (red). The first ANS molecule is depicted by solid lines and the second ANS molecule by dotted lines. Atom numbering is indicated in the chemical structure. **b)** Root mean square deviation of all Cα atoms resulting from the superposition of apo-CDK2 with the CDK2-ANS complex (red), of CDK2-ANS-JWS648 with CDK2-ANS (green), and of CDK2-ANS-SU9516 with CDK2-ANS.

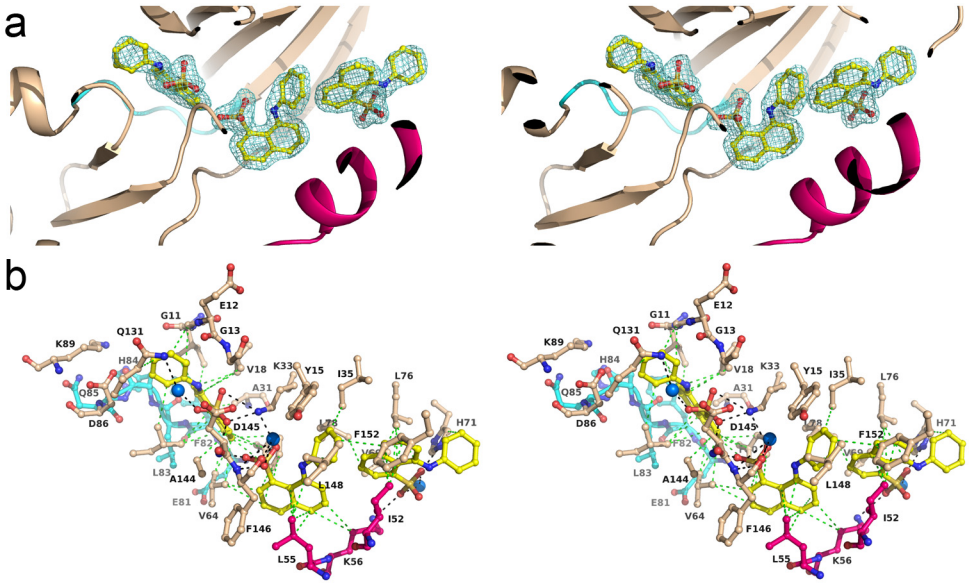

Supplementary Figure 3 Structure determination of apo-CDK2 crystals upon prolonged in-diffusion with 15 mM ANS reveals a third ANS molecule bound loosely to the ATP site. **a)** Stereoview of three ANS molecules bound to CDK2. Displayed in blue is the 2Fo-Fc electron density, contoured at 1σ around the ANS molecules. The Fo-Fc electron density map with the ANS molecules omitted during refinement is shown in **Supplementary Figure 7d**. The C-helix is shown in pink and the hinge region in cyan. **b**) Stereoview of binding interactions between the three ANS molecules and CDK2 residues. Black and green dotted lines indicate hydrogen bonding and hydrophobic interactions, respectively. Water molecules are shown as blue spheres.

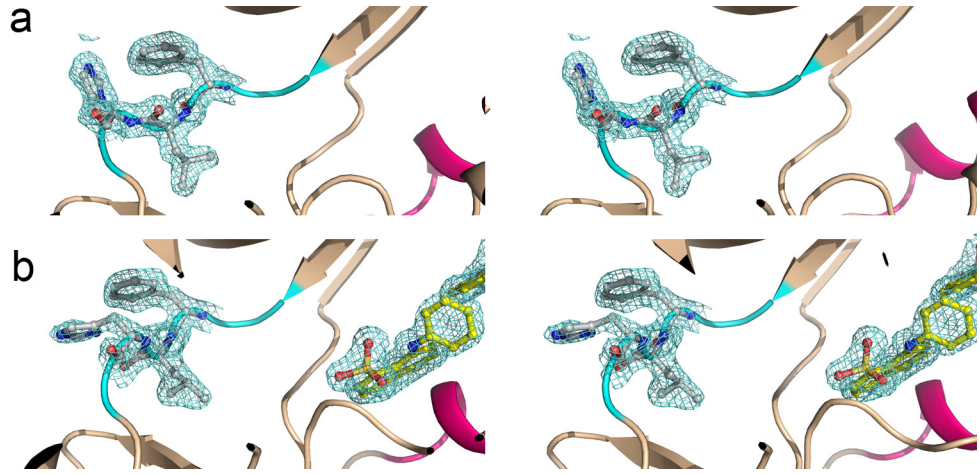

Supplementary Figure 4 Conformational changes in the hinge region of the ATP site induced upon binding of ANS to the allosteric site. **a**) Stereoview of the hinge region in apo-CDK2 with the 2Fo-Fc electron density contoured at 1σ for residues Phe82, Leu83, and His84. **b**) Stereoview of the hinge region in the binary CDK2-ANS complex with the 2Fo-Fc electron density contoured at 1σ for the same residues.

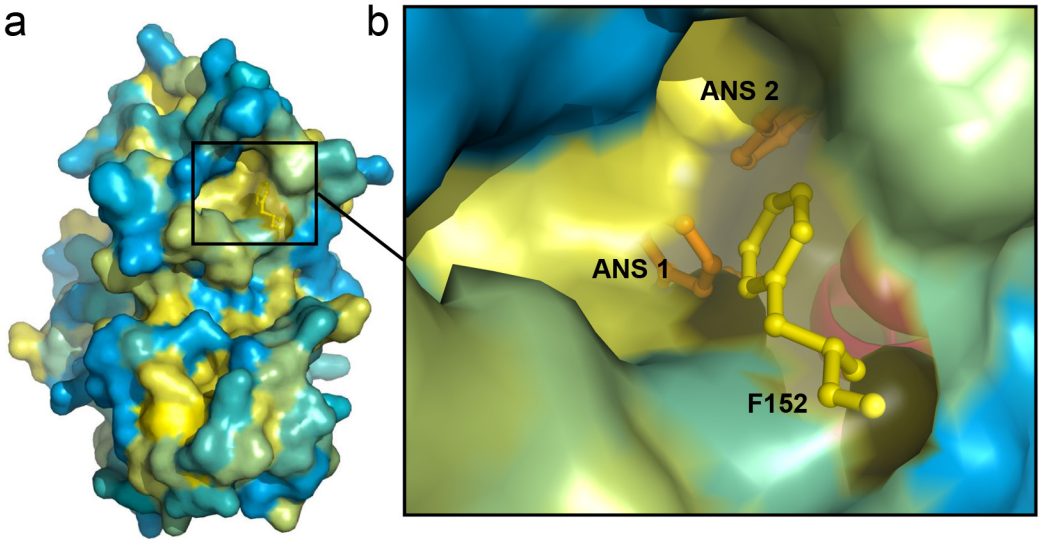

Supplementary Figure 5 Potential entry site of ANS into apo-CDK2. **a)** Van der Waals surface according to residue polarity, from blue (hydrophilic) to yellow (hydrophobic). **b)** Detailed view of the hydrophobic pocket surrounding Phe152 with the two ANS molecules superimposed.

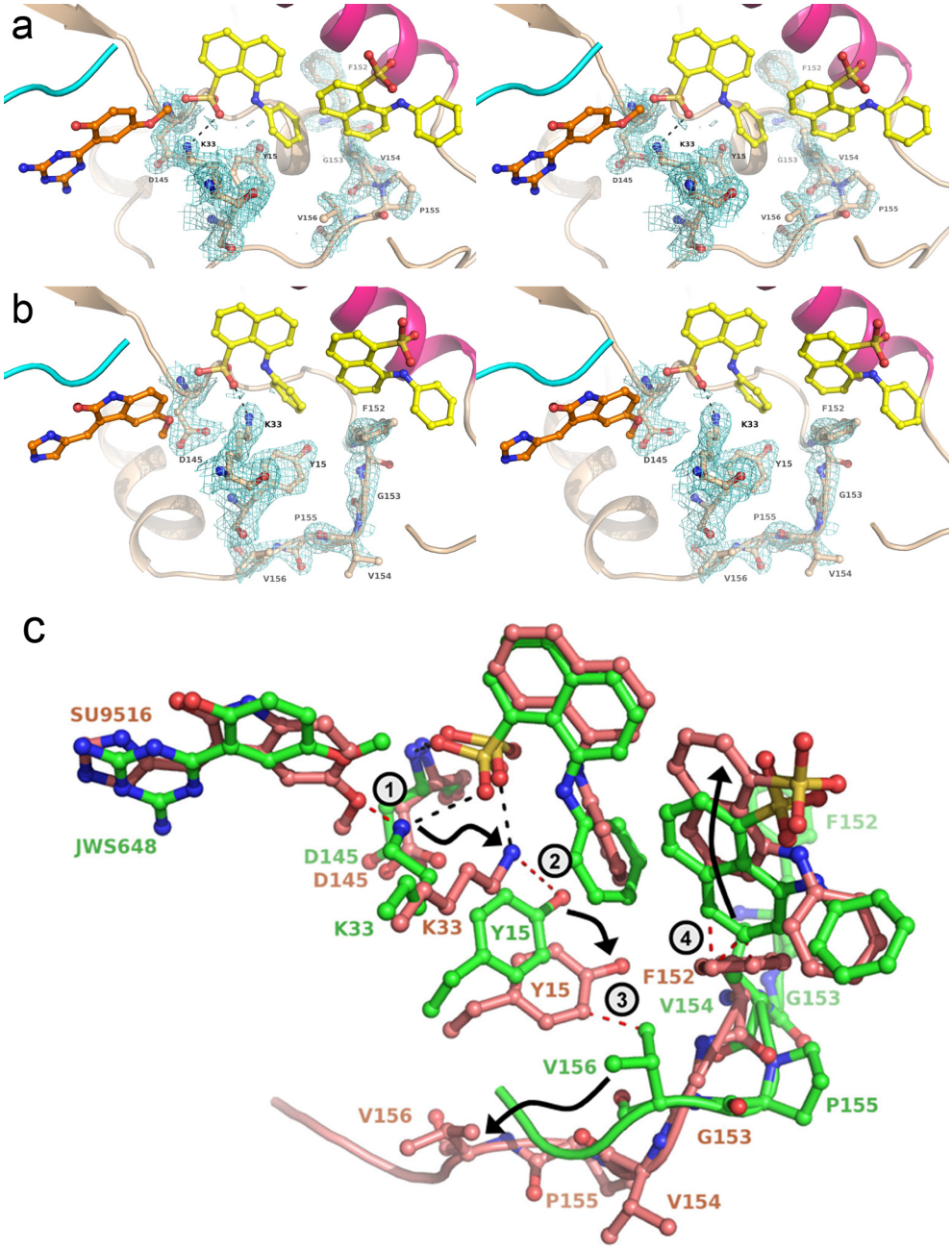

Supplementary Figure 6 Conformational changes induced by SU9516 in complex with ANS. **a)** Stereoviews of the CDK2-ANS-JWS648 complex and **b)** the CDK2-ANS-SU9516 complex, with the 2Fo-Fc electron density displayed around Lys33 and neighboring residues, as well as residues 152–156 of the activation loop. **c)** Superimposition of CDK2-ANS-JWS648 (green) and CDK2-ANS-SU9516 (salmon). Observed conformational changes are indicated by black arrows and are numbered 1–4.

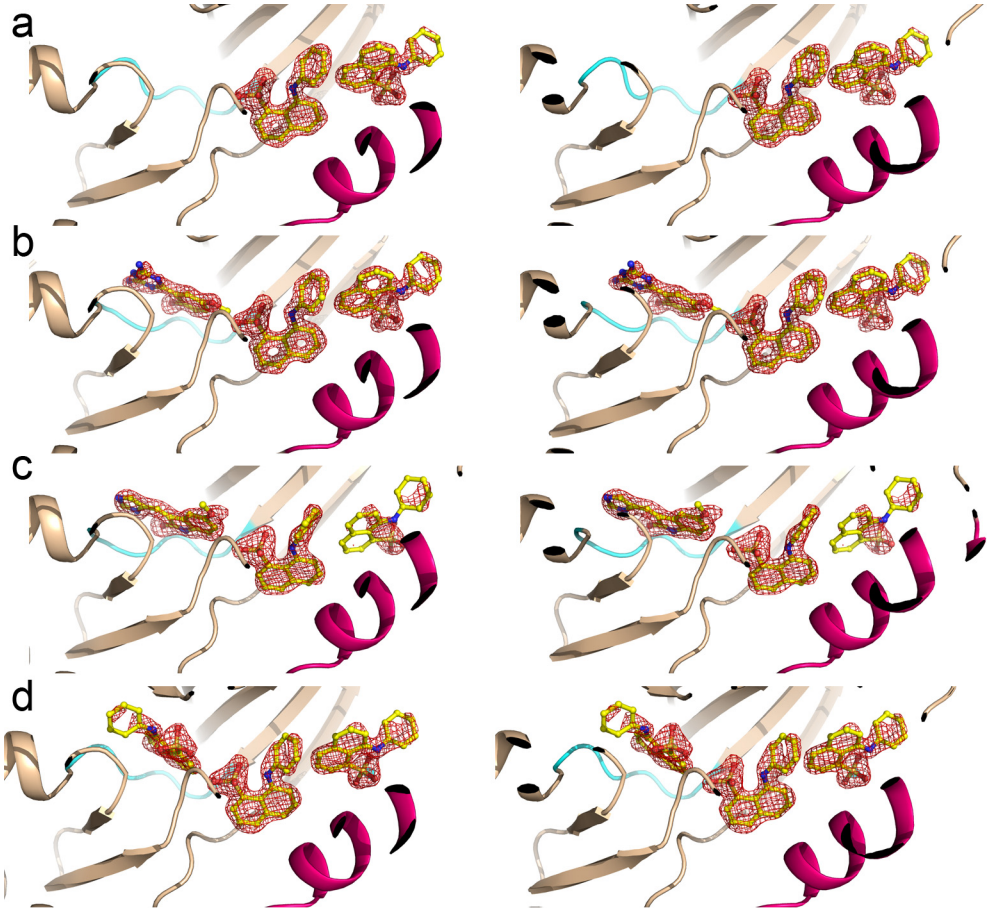

Supplementary Figure 7 Fo-Fc electron density contoured at 3σ as a result of refinement cycles (annealing and B-factor refinement) omitting the respective ligands. **a**) CDK2-ANS, **b**) CDK2-ANS-JWS648, **c**) CDK2-ANS-SU9516, and **d**) CDK2-ANS upon in-diffusion of 15 mM ANS into apo-CDK2 crystals